Analog of superradiant emission in thermal emitters

Ming Zhou,[1] Soongyu Yi,[1] Ting Shan Luk,[2] Qiaoqiang Gan,[3] Shanhui Fan,[4] and Zongfu Yu[1]
[1]*Department of Electrical and Computer Engineering, University of Wisconsin-Madison, Wisconsin 53706, USA*
[2]*Sandia National Laboratories, Albuquerque, New Mexico 87185, USA*
[3]*Department of Electrical Engineering, The State University of New York at Buffalo, Buffalo, New York 14260 USA*
[4]*Department of Electrical Engineering and Ginzton Lab, Stanford University, Stanford, California 94305 USA*
(Received 29 June 2014; revised manuscript received 7 May 2015; published 13 July 2015)

When wave effects of thermal photons become significant, thermal emitters can exhibit intriguing coherent effects. Here, we show that the superradiant emission, which was originally found in quantum emitters, can be realized in resonant thermal emitters. Similar to the superradiance in quantum emitters, the in-phase oscillation of resonant emitters reduces the lifetime of thermal photons in the emitters. Unlike the atomic superradiance, one remarkable consequence of the thermal superradiance is the anomalous power scaling, where the emission power can scale inversely with the number of thermal emitters. More thermal emitters generate less power due to the coherent interference of thermal photons.

DOI: 10.1103/PhysRevB.92.024302 PACS number(s): 78.67.Pt, 44.40.+a, 78.20.Ci, 42.72.Ai

Nanophotonic control of thermal emission [1,2] has attracted significant recent interest because of potential applications in areas such as thermophotovoltaics [3–8], lighting [9], and radiative cooling [10,11]. From a fundamental physics perspective, with the capability to tailor light-matter interactions, nanophotonic structures can enable thermal emission behaviors that are drastically different from those of conventional bulk emitters [12–23]. For example, while blackbody emitters are typically considered to be incoherent with a total emission power limited by the Stefan-Boltzmann law, nanophotonic emitters can be highly coherent [6,20,22] or have emission beyond the blackbody limit [4,19].

In this paper, we consider thermal emission from resonant nanophotonic emitters, placed in close proximity with the spacing between the emitters at deep subwavelength scale. We show that such emitters can exhibit counterintuitive thermal radiation behaviors. In particular, while the conventional wisdom would have predicted that the total power from N identical thermal emitters increases linearly with N, here we show that the coherent interaction can result in anomalous scaling with respect to N. Under the right condition, the power in fact can scale as $1/N$. We identify this effect associated with the $1/N$ scaling as the thermal analog of the superradiance effect (Fig. 1).

The superradiance effect was discovered in the study of spontaneous emission for N identical two-level quantum emitters. In 1954, Dicke discovered the superradiance [24] effect: The intensity of the total emission scales as N^2 when N emitters are placed together in a subwavelength volume, rather than N as one may expect with the emitters being treated as independent. Superradiance is a direct consequence of the wave effect uniquely found in subwavelength dimensions. When placed in a subwavelength volume, the emission process results from a collective in-phase oscillation of the resonant transitions, which reduces the radiative lifetime of the excited state of the quantum emitters. Shorter radiative lifetime directly leads to more intense emission during the transient process of the decay of the excited state. The superradiance has been an active field in atomic physics for decades [25–27]. Recently, it has also been studied in classical optics in the context of electromagnetically induced transparency [28,29], Fano interference [30–32], and in complex radiation environments [33–36].

The analog of superradiance has never been considered to be present in thermal emitters, which is vaguely justified since the underlying process of thermal radiation is an incoherent process. At first glance, this observed thermal superradiance effect in this paper, which results in a suppression of emission as the number of emitters increases, appears significantly different from the enhancement effect observed in the superradiance of quantum emitters. We will show that such different scaling with respect to the number of emitters originates from the same underlying physics, i.e., the in-phase superposition of the resonant decay. The requirements to observe the thermal superradiance are closely related to the requirements for observing quantum superradiance: The thermal emitters must support optical resonance, and these resonant emitters must be placed in a deep subwavelength dimension as shown in Fig. 1(b). For the organization of the paper, we will first use direct numerical simulations to provide concrete examples of the thermal superradiance. Then we will develop analytical theory to illustrate the physical mechanism.

We start with the simulation of thermal emission of ordinary nonresonant emitters, such as a block of emissive material in the free space as shown in Fig. 2(a). A finite-element method is used to solve the frequency-domain Maxwell's equations in a two-dimensional (2D) space. Electric current sources of random phases, represented by black dots, are randomly placed in the emitters to simulate the emission process (see the Supplemental Material for further details [37]). Figures 2(b) and 2(c), which use the same color map, show the intensity distribution of the emission from one and five emitters, respectively. The emission power simply grows by five times for five emitters.

In order to observe the superradiant thermal emission, we place several resonant emitters in a subwavelength dimension. This requirement is difficult to satisfy for most dielectric resonators since their sizes are comparable to the wavelength. To overcome the size limitation, our numerical example is based on ultracompact electromagnetic resonance found in deep subwavelength slits as shown in Fig. 2(d). The slit is created in a slab of perfect electric conductor (PEC). The

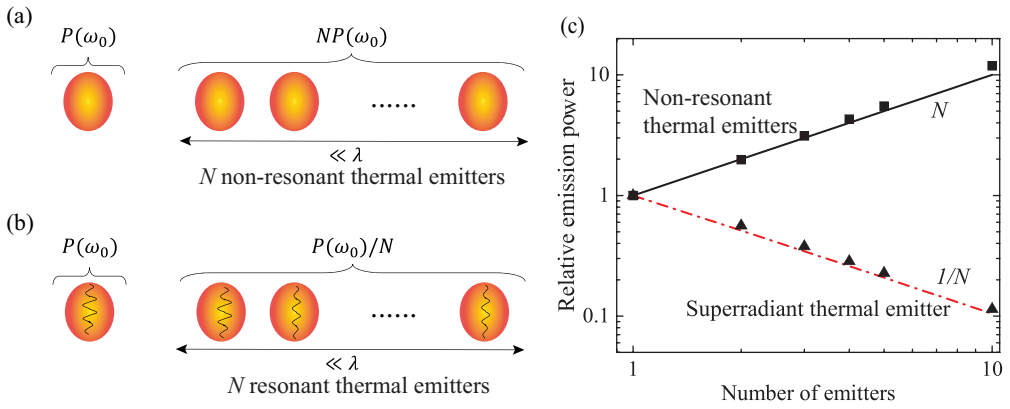

FIG. 1. (Color online) (a) Schematic of nonresonant thermal emitters. The total power from N emitters is N times that of a single emitter alone. (b) Schematic of superradiant resonant thermal emitters. The total power scales as $1/N$ at the resonant frequency. (c) The emission power of N emitters, normalized by the power of a single emitter alone. The solid line is for nonresonant thermal emitters, indicating a linear scaling $\sim N$; the dashed line $\sim 1/N$ is for superradiant resonant emitters. Lines are from analytical theory while markers are simulation results obtained from full-wave Maxwell's equations.

reflection at the openings of the slit creates a Fabry-Perot (FP) cavity. The optical fields are tightly confined in the slit. When filled with absorptive dielectric materials, the slit becomes a resonant thermal emitter. More details of the resonator are presented in the Supplemental Material [37].

The emission of a single slit has a characteristic Lorentz line shape as shown by the emission cross section plotted in Fig. 2(e). The spatial profile of the emission at the resonant frequency is shown in Fig. 2(f). When five slits are closely placed together, the emission power reduces by five times, which can be clearly seen in both the spatial profile [Fig. 2(g)] and the spectrum of emission cross section [Fig. 2(h)]. We simulate the emission power for $N = 1$, 2, 3, 4, 5, and 10 emitters for both nonresonant and resonant thermal emitters. As shown in Fig. 1(c), the total emission power of nonresonant emitters (square markers) increases linearly with N while that of the resonant emitters falls nicely on a $1/N$ relation (triangular markers). Such anomalous power scaling is a direct consequence of the in-phase oscillation, which shares the same physical mechanism as the superradiance of quantum emitters.

Next, we develop an analytical theory to describe the collective thermal emission from N emitters, as observed

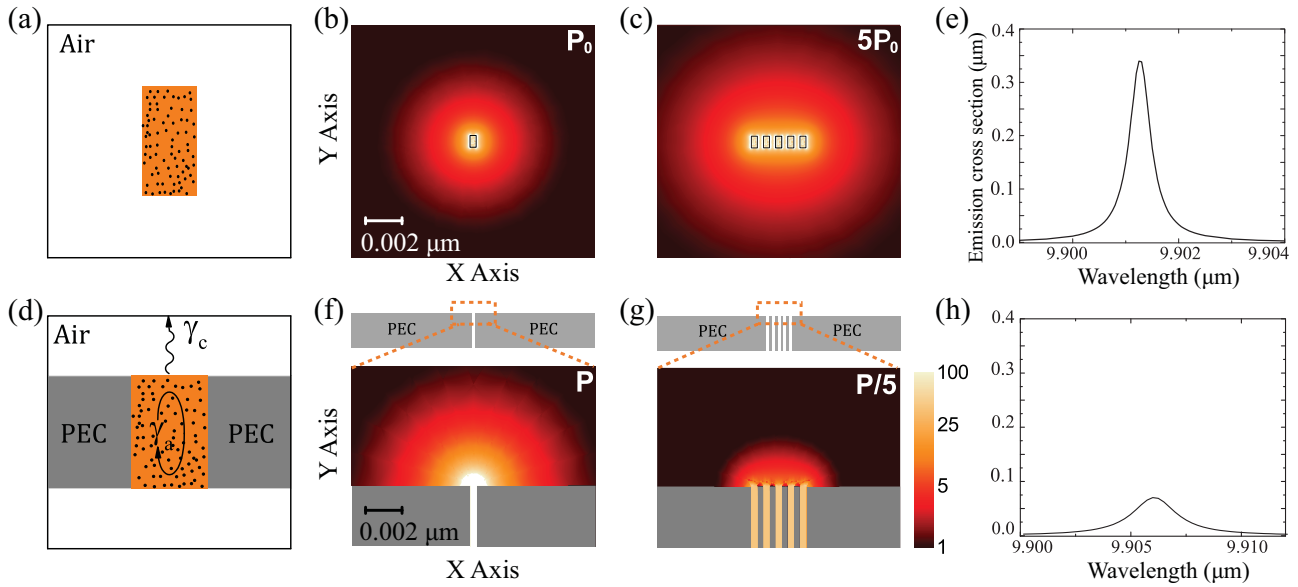

FIG. 2. (Color online) (a) The structure of a nonresonant emitter: a block of emissive materials. Random positioned current sources (black dots) with random phases are used to simulate the thermal emission. (b, c) Intensity distribution of the emission at a wavelength of 9.9 μm for one and five nonresonant emitters, respectively. (d) The structure of resonant emitters consisting of a slit in a PEC slab. The length and width of the slit are 1.4 μm and 0.5 nm, respectively. It is filled with an emissive material with a dielectric constant of $\epsilon = 12.5 + 0.000\,01i$. The resonator is in the overcoupling region. (e) Spectra of emission cross section for one resonant emitter. The emission cross section is calculated by integrating the absorption cross section over all angles and also by considering the reciprocal relation between the absorption and the emission. (f, g) Distribution for one and five emitters, respectively. Simulation is performed for transverse magnetic (TM) modes since the nonresonant transverse electric (TE) polarization has negligible contribution. (h) Spectra of emission cross section for five resonant emitters.

in the aforementioned simulations. Based on the coupled mode theory [38], we represent the amplitudes of thermal electromagnetic fields stored in the resonant emitters as $\mathbf{a} = (\mathrm{a}_1, \mathrm{a}_2, \ldots, \mathrm{a}_N)^T$; a_i is normalized such that $|\mathrm{a}_i|^2$ is the energy stored in the ith emitter. The amplitude of each resonant emitter may decay through two pathways. The first pathway is to escape to the far field as emission, which is described by the coupling rate γ_c [Fig. 2(d)]. The second is to get absorbed by the absorptive material inside the slit, which is described by the absorption rate γ_a [Fig. 2(d)]. In the framework of the fluctuation-dissipation theorem, such absorption process is balanced by a random thermal excitation source. With all these considerations, the amplitudes are governed by the following equation:

$$\frac{d}{dt}\mathbf{a} = \left[\left(j\omega_0 - \frac{\gamma_a}{2} - \frac{\gamma_c}{2}\right)\boldsymbol{I} - \boldsymbol{\Gamma}\right]\mathbf{a} + \sqrt{\gamma_a}\mathbf{n}\,, \qquad (1)$$

where $\boldsymbol{I}$ is a $N \times N$ identity matrix, ω_0 is the resonant frequency (here we assume all resonant emitters have the same resonant frequency), and $j = \sqrt{-1}$. The thermal excitation source $\mathbf{n}$ satisfies [39]

$$\langle \mathrm{n}_i^*(\omega)\mathrm{n}_j(\omega')\rangle = \frac{1}{2\pi}\frac{\hbar\omega}{e^{\hbar\omega/k_BT} - 1}\delta(\omega - \omega')\delta_{i,j}, \qquad (2)$$

where $\hbar$ and k_B are the reduced Planck's constant and Boltzmann constant, respectively. ω and ω' are the angular frequencies. T is the temperature, and δ is the delta function. i, j represent sources in the emitters i and j, respectively.

What enables the superradiant effect is the indirect interaction among resonant emitters represented by $\boldsymbol{\Gamma}$. Resonant emitters separated by deep-subwavelength spacing emits with the same far-field radiation pattern, and hence the emissions can interfere with each other, result in the indirection interaction [38]. It is completely different from the direct interaction created by the overlapping near fields [40], which cause the hybridization of resonators [41]. To obtain the explicit form of $\boldsymbol{\Gamma}$, we need to quantify the coupling between resonators and the free-space far fields. For this purpose, we model the free space with a set of orthogonal radiation channels $\mathbf{S}$. Here we focus on a 2D space. Each channel represents a plane wave propagating in a distinct direction in the angle θ_i (Fig. 3). It is normalized such that each element $|\mathrm{S}_i|^2$ represents the power carried by the channel. There are infinite directions in the free space. To treat this infinity, we start with a space that is finite in the x direction with a length L, and impose a periodic boundary condition at the edge of such space. We then take the $L \to \infty$ limit to recover the infinite case. The ith channel is characterized by a wave vector with a parallel component $k_i^{\parallel} = 2\pi i/m\lambda_0$, where λ_0 is the resonant wavelength and index $i = -m, m \ldots, 0, \ldots,$ and $m = L/\lambda_0$ (Fig. 3). The resonators emit to the channels according to

$$\mathbf{S} = \begin{pmatrix} \boldsymbol{D}^{\mathbf{up}} \\ \boldsymbol{D}^{\mathbf{low}} \end{pmatrix}\mathbf{a} = \boldsymbol{D}\mathbf{a}, \qquad (3)$$

where $\boldsymbol{D}^{\mathbf{up}}$, $\boldsymbol{D}^{\mathbf{low}}$ are $(2m+1) \times N$ matrices, responsible for channels in the upper and the lower half spaces, respectively. $D_{i,j}$ represents the coupling rate from the jth emitter to the ith channel. Since emitters are spaced by a distance much smaller than the wavelength, the couplings to the channels are identical

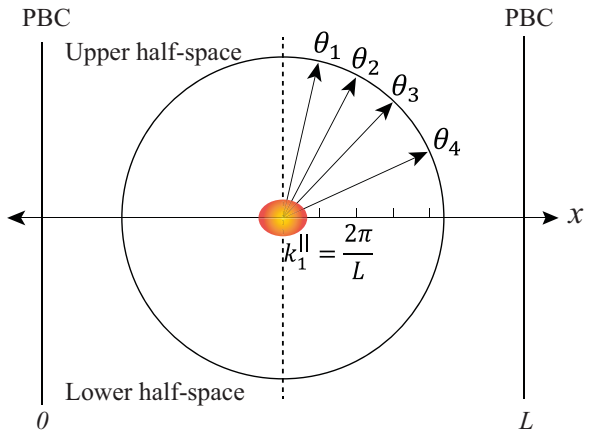

FIG. 3. (Color online) Schematic of the orthogonal radiation channels. An emitter is located within two boundaries where periodic boundary condition (PBC) is applied. The infinite nonperiodic case will be obtained by taking the period $L \to \infty$.

[42,43]. We further assume an isotropic emission profile for each emitter. Then we can write the elements of $\boldsymbol{D}^{\mathbf{up}}$ and $\boldsymbol{D}^{\mathbf{low}}$ as

$$\boldsymbol{D}^{\mathbf{up}}_{i,j} = \boldsymbol{D}^{\mathbf{low}}_{i,j} = \sqrt{\frac{\gamma_c}{2m\pi\cos\theta_i}}\,, \qquad (4)$$

where $\theta_i = \arcsin(i/m)$.

By applying the energy conservation [38] (see the Supplemental Material [37] for further details), we can obtain the specific form of $\boldsymbol{\Gamma}$,

$$\Gamma_{i,j} = \tfrac{1}{2}\gamma_c(1 - \delta_{i,j}).$$

The form of $\boldsymbol{\Gamma}$ shows that an isotropic indirect interaction is induced among all resonant emitters with equal strength. Such indirect interaction only exists when emitters are placed in a deep subwavelength dimension. When the spacing increases, a phase delay has to be introduced, resulting in nonisotropic indirect interaction and weakened superradiance [40].

With $\boldsymbol{\Gamma}$, we can explicitly calculate $\mathbf{a}(\omega)$ in the frequency domain

$$\mathbf{a}(\omega) = \left[\left(j(\omega - \omega_0) + \frac{\gamma_a}{2} + \frac{\gamma_c}{2}\right)\boldsymbol{I} + \boldsymbol{\Gamma}\right]^{-1}\sqrt{\gamma_a}\,\mathbf{n}(\omega). \qquad (5)$$

The power spectral density of the emission $P(\omega,\theta)$ is related to $\mathbf{a}(\omega)$ by (see the Supplemental Material [37] for detailed derivation)

$$P(\omega,\theta) = \sum_{i=1}^{N}\sum_{k=1}^{N}\int_0^{\infty}\frac{\gamma_c}{2m\pi\cos\theta}e^{-j(\omega-\omega')t}\langle \mathrm{a}_i^*(\omega)\mathrm{a}_k(\omega')d\omega'\rangle. \qquad (6)$$

Combining Eqs. (5) and (6) and Eq. (2), we obtain the power spectral density as [44]

$$P(\omega,\theta) = \frac{1}{2\pi}\frac{\hbar\omega}{e^{\hbar\omega/k_BT} - 1}\frac{N\gamma_a\gamma_c}{(\omega - \omega_0)^2 + \left(\frac{N\gamma_c+\gamma_a}{2}\right)^2} \times \frac{1}{2m\pi\cos\theta}. \qquad (7)$$

This equation involves the number of channels m, which becomes infinite at $L \to \infty$. To cancel m, we consider the emission cross section $\sigma(\omega,\theta)$:

$$\sigma(\omega,\theta) = \frac{P(\omega,\theta)}{\frac{1}{2\pi L\cos\theta}\frac{\hbar\omega}{e^{(\hbar\omega/k_BT)}-1}} = \frac{\lambda}{2\pi}\frac{N\gamma_a\gamma_c}{(\omega-\omega_0)^2+\left(\frac{N\gamma_c+\gamma_a}{2}\right)^2}. \quad (8)$$

The normalization factor $\hbar\omega/[2\pi L\cos\theta(e^{\hbar\omega/k_BT}-1)]$ is the power flux density in a single channel [45]. The emission cross section has a Lorentz line shape, which agrees with the simulation.

The total emission power can be obtained by multiplying the angle-integrated cross section by the blackbody spectral density:

$$P(\omega) = \frac{\omega}{4\pi^2 c}\frac{\hbar\omega}{e^{\hbar\omega/k_BT}-1}\int\sigma(\omega,\theta)d\theta = \frac{1}{2\pi}\frac{\hbar\omega}{e^{\hbar\omega/k_BT}-1}\frac{N\gamma_c\gamma_a}{(\omega-\omega_0)^2+(\frac{N\gamma_c+\gamma_a}{2})^2}. \quad (9)$$

Here c is the speed of light in vacuum. Equation (9) is the main result of the theory. When $N = 1$, Eq. (9) reproduces the emission of a single resonant emitter derived in [39]. It is straightforward to recover the results of ordinary nonresonant emitters by taking the frequency far away from the resonance, i.e., $|\omega-\omega_0| \gg N\gamma_c+\gamma_a$. As expected, the emission power $P(\omega) \approx \frac{1}{2\pi}\frac{\hbar\omega}{e^{\hbar\omega/k_BT}-1}\frac{\gamma_c\gamma_a}{(\omega-\omega_0)^2}N$ scales linearly with N.

The superradiant effect is most prominent when the coupling rate is much larger than the absorption rate, i.e., $\gamma_c \gg \gamma_a$. In this case, each thermally generated photon spreads equally among N emitters with the same phase because of the strong isotropic indirect interaction $\mathbf{\Gamma}$. For a direct visualization, Fig. 4(a) shows the simulated amplitude distribution of the electromagnetic field generated by a single point source placed in one of the slits. The field is evenly distributed among all slits with an identical phase. More importantly, the uniform phase distribution occurs regardless of the location of the source. Because any thermal photon evenly occupies all slits, the effective coupling rate to the far field increases by N times and thermal photons decay much faster. Consequently, the emission power is suppressed:

$$P_N(\omega_0) \approx \frac{2\hbar\omega_0}{\pi(e^{\hbar\omega_0/k_BT}-1)}\frac{\gamma_a}{\gamma_c}\frac{1}{N}, \quad (10)$$

which scales inversely with N.

The superradiant effect disappears when the coupling rate is much smaller than the absorption rate, i.e., $\gamma_c \ll \gamma_a$. In this case, the thermal photon is mostly confined in the emitter where its source is located. Here, we increase the imaginary part of the dielectric constant of the lossy material in the slit such that $\gamma_a = 100\gamma_c$. Figure 4(b) shows the simulated amplitude distribution of the electromagnetic field generated by a single point source placed in one of the slits. In contrast to Fig. 4(a), in this case the amplitude of the field is mostly confined only in the slit where the source is located. Consequently, the presence of other slits does not have any effect on the emission of the source. Therefore, when filled with very lossy materials, the slits emit independently. The total emission power is a simple linear addition. This is again supported by the theory. We take $\gamma_a \gg \gamma_c$ in Eq. (9) and obtain

$$P_N(\omega_0) \approx \frac{2\hbar\omega_0}{\pi(e^{\hbar\omega_0/k_BT}-1)}\frac{\gamma_c}{\gamma_a}N, \quad (11)$$

which scales linearly with N. Figure 4(c) shows the spectra of the emission cross section for very lossy materials where five emitters (dashed red line) simply emit five times more power than the single emitter (black solid line). The insets show the intensity distribution of emission for a single (left) and five emitters (right). These results are in great contrast to the superradiant power scaling shown in Figs. 2(e) and 2(f) despite the fact that both cases are resonant emitters.

The superradiant effect also gradually disappears as the interemitter distance increases. In the coupled mode theory, when interemitter distance is above the resonant wavelength, the indirect interaction $\mathbf{\Gamma}$ greatly decreases [43] because emitters start to radiate to different far-field modes. In this case, the emission power scales linearly with the number of emitters N. In the simulations, we calculate the emission power of five resonant slits with an increasing interemitter distance shown in Fig. 4(d). The superradiant suppression of emission is only observed when the distance is in the deep subwavelength regime. When the distance gradually increases to a few micrometers, the emission power approaches five times that of a single emitter. Also consistent with the characteristic feature of the linear power scaling, the field distribution for a thermal photon becomes more and more confined in an individual slit when the distance increases [not shown in Fig. 4(d)].

Next, we illustrate the connection and difference between the superradiance of thermal and quantum emitters. The power suppression in thermal superradiance seems to contradict the enhanced emission intensity observed in the spontaneous superradiance of quantum emitters. To understand the difference, it is important to note that the spontaneous emission of quantum emitters is measured in the time domain. For N excited two-level systems (for simplicity, suppose there is no nonradiative recombination) arranged in a superradiant configuration, the total number of photons emitted *cannot* be enhanced, and it is always N. The superradiance makes the emitters decay N times faster. Therefore emitters look brighter in the transient decay process. But the emission lasts for a shorter period of time and it is darker than the single emitter alone after the initial period of the decay as shown in Fig. 5(a).

On the other hand, the thermal emission is always measured in the steady-state frequency domain where the emitter is maintained at a constant temperature T. The shorter decay time caused by the superradiant in-phase oscillation does not lead to the apparent enhancement of the emission intensity. Instead, the signature of superradiance, i.e., the faster decay, is manifested as the N-times broadened bandwidth, which is clearly shown in Figs. 2(e) and 2(h), and Eq. (9). If the thermal emission were to be measured in the time domain, we would also observe the same N^2 enhancement in the transient process. To show this enhancement, we consider a thought experiment. At time $t = 0$, a resonant thermal emitter is prepared at temperature T in a vacuum space filled with zero-temperature radiation fields. Let us further assume that emitters

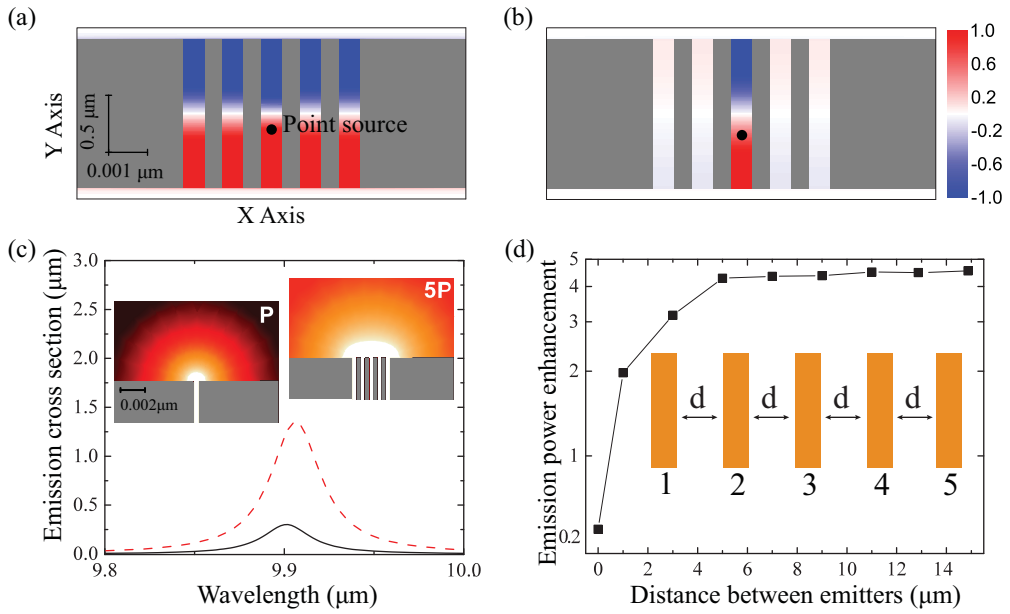

FIG. 4. (Color online) (a) When the absorption rate is low, a point source excites photons with equal amplitudes and phases in all emitters. Color shows the amplitude of the electric field. (b) When the absorption is high, excited amplitude is localized in the slit with the source. (c) Quench of the superradiance effect in the high-loss regime. Spectra of the emission cross section of a single (black solid line) and five (red dashed line) resonant emitters. Insets are the intensity distribution of the emission. (d) The emission power as a function of distance between emitters in the low-loss regime. It is normalized by the power generated by a single emitter alone. The superradiance effect is weakened as the interemitter distance increases.

have infinitesimally small heat capacity so that when thermal photons leave, the emitter's temperature drops instantaneously. This setting helps to observe the transient process. The time-dependent emission of a single emitter is shown by the black line in Fig. 5(b). The number of thermal photons starts from $1/[\exp(\hbar\omega/k_BT) - 1]$ and exponentially decays to zero. If we prepare three such thermal emitters separately and then bring them together in a superradiant configuration, they decay three times faster. Further assisted by a factor of 3 due to more available thermal photons, the transient emission intensity increases by nine times [red line in Fig. 5(b)]. Here the time-domain calculation based on the coupled mode theory shows that the enhancement of transient emission of thermal emitters indeed is the same as quantum emitters.

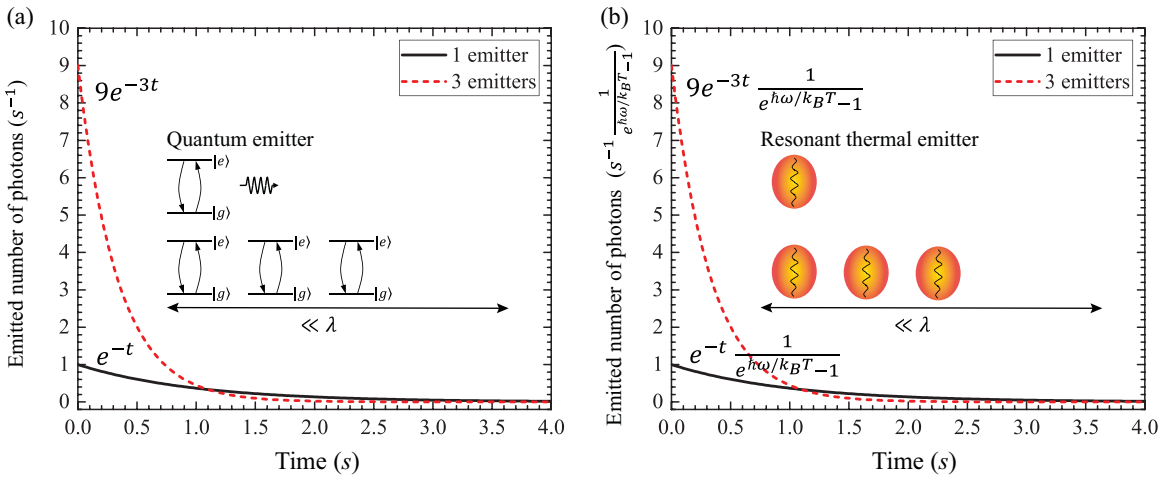

FIG. 5. (Color online) (a) The emitted number of photons flux from quantum emitters as a function of time in the transient decay process. The lifetime of photons is assumes to be 1 s. A single quantum emitter is shown as a black solid line. When three such quantum emitters are placed together (dashed red line), the total number of photons is tripled, and the lifetime of photons is reduced to 1/3 s. As a result of more photons and faster decay, the initial intensity from the emitters is enhanced at $t = 0$ and drops faster below the black line at a later time. (b) Emitted thermal photons as a function of time for single (black line) and three (red dashed line) resonant thermal emitters. For three resonant thermal emitters in a superradiant configuration, the decay rate increases three times. The thermal emission increases nine times at $t = 0$, which is the same as the case of quantum emitters.

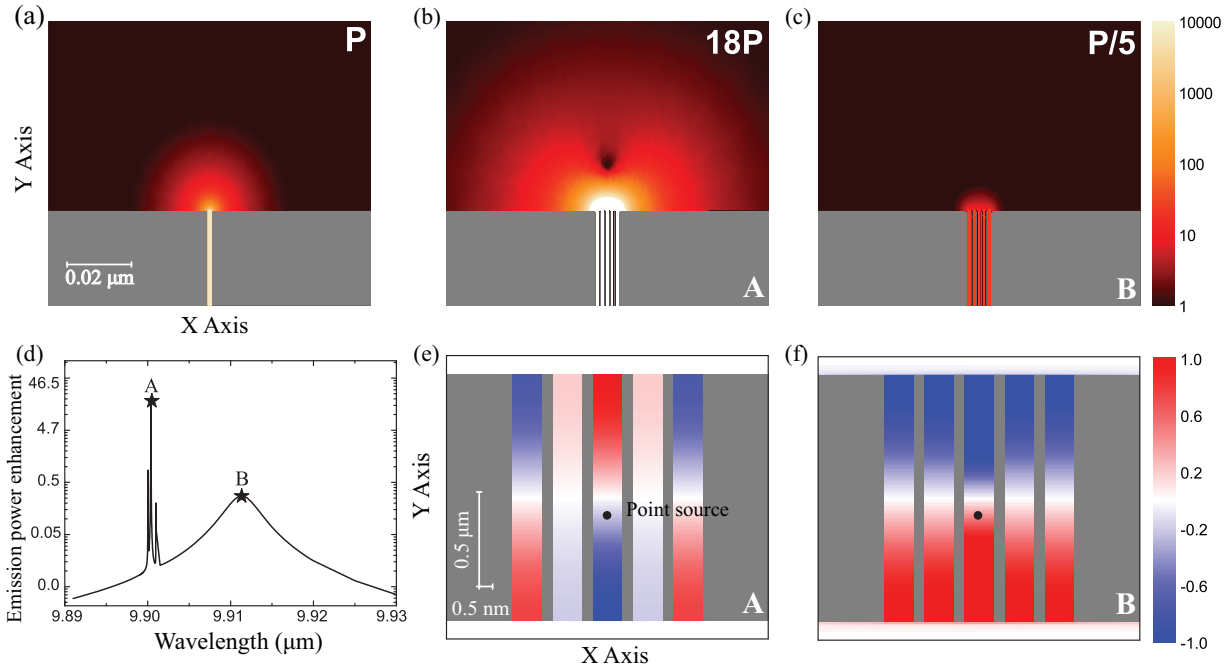

FIG. 6. (Color online) (a) Intensity distribution of the emission from a single emitter. (b, c) Intensity distribution of the emission from five emitters at the subradiant mode (b) and the superradiant mode (c), respectively. (d) The spectrum of the emission power for five emitters, normalized by the peak power of a single emitter. (e, f) The amplitude of the electric field excited by a point source in one of the slits for the subradiant mode (e) and the superradiant mode (f), respectively.

Lastly, instead of the $1/N$ scaling behavior as we have discussed in most of the paper, with proper design we can also achieve other scaling behaviors as well. For example, we can design a system in which the total emission power scales superlinearly as a function of N. When the thermal photons have opposite phases in different emitters, the decay of the thermal photons to the free space can be made slower. These modes have a narrower bandwidth than a single emitter. The emission power can be significantly enhanced.

To create opposite phase distribution, we rely on the near-field interaction, which hybridizes the eigenmodes [40,41]. The near-field interaction can be introduced by using wider slits where optical fields are less confined locally [Fig. 6(a)]. The spectrum of emission cross sections of five resonant emitters are shown in Fig. 6(d) in the log scale. The main broad peak remains the superradiant state with five-times suppressed emission as shown by peak B in Figs. 6(d) and 6(c). Additionally, there are a few sharp emission peaks far away from the main resonant frequency because the hybridization shifts the frequencies of these states. For peak A in Fig. 6(d), the emission power is enhanced by 18 times and its emission distribution is shown in Fig. 6(b). This power calculation is indeed consistent with the prediction based on the phase configuration of the mode. For peak A, the phases of thermal photons are opposite as shown in Fig. 6(e), which is in great contrast to the superradiant in-phase oscillation shown in Fig. 6(f). These emission properties could be useful for engineering thermal radiation for efficient energy conversion devices.

In conclusion, we theoretically demonstrated that superradiance exists in thermal emitters and verified it by numerical simulation. The superradiant effect in thermal emitters leads to abnormal power scaling; i.e., the radiation power is inversely proportional to the number of emitters, which is in great contrast to the quadratic power scaling in superradiant quantum emitters. Such emission behavior provides more understanding of thermal emission at nanoscale, and could be useful for engineering thermal radiation for efficient energy conversion devices.

The authors thank Linxiao Zhu for useful discussion. Support for this research was provided by the Office of Naval Research under Grant No. N00014-14-1-0300 and by the Wisconsin Alumni Research Foundation. S.F. is supported by the DOE "Light-Material Interactions in Energy Conversion" Energy Frontier Research Center under Grant No. DE-SC0001293.

[1] M. Laroche, R. Carminati, and J.-J. Greffet, Phys. Rev. Lett. **96**, 123903 (2006).
[2] E. Rousseau, A. Siria, G. Jourdan, S. Volz, F. Comin, J. Chevrier, and J.-J. Greffet, Nat. Photonics **3**, 514 (2009).
[3] S. Y. Lin, J. Moreno, and J. G. Fleming, Appl. Phys. Lett. **83**, 380 (2003).
[4] A. Narayanaswamy and G. Chen, Appl. Phys. Lett. **82**, 3544 (2003).

[5] P. Nagpal, S. E. Han, A. Stein, and D. J. Norris, Nano Lett. **8**, 3238 (2008).
[6] E. Rephaeli and S. Fan, Opt. Express **17**, 15145 (2009).
[7] R. Messina and P. Ben-Abdallah, Sci. Rep. **3**, 1383 (2013).
[8] A. Lenert, D. M. Bierman, Y. Nam, W. R. Chan, I. Celanović, M. Soljačić, and E. N. Wang, Nat. Nanotechnol. **9**, 126 (2014).
[9] J.-J. Greffet, Nature **478**, 191 (2011).
[10] E. Rephaeli, A. Raman, and S. Fan, Nano Lett. **13**, 1457 (2013).
[11] A. P. Raman, M. A. Anoma, L. Zhu, E. Rephaeli, and S. Fan, Nature **515**, 540 (2014).
[12] A. V. Shchegrov, K. Joulain, R. Carminati, and J.-J. Greffet, Phys. Rev. Lett. **85**, 1548 (2000).
[13] M. U. Pralle, N. Moelders, M. P. McNeal, I. Puscasu, A. C. Greenwald, J. T. Daly, E. A. Johnson, T. George, D. S. Choi, I. El-Kady, and R. Biswas, Appl. Phys. Lett. **81**, 4685 (2002).
[14] J.-J. Greffet, R. Carminati, K. Joulain, J.-P. Mulet, S. Mainguy, and Y. Chen, Nature **416**, 61 (2002).
[15] I. Celanovic, D. Perreault, and J. Kassakian, Phys. Rev. B **72**, 075127 (2005).
[16] M. Laroche, C. Arnold, F. Marquier, R. Carminati, J.-J. Greffet, S. Collin, N. Bardou, and J.-L. Pelouard, Opt. Lett. **30**, 2623 (2005).
[17] B. J. Lee, C. J. Fu, and Z. M. Zhang, Appl. Phys. Lett. **87**, 071904 (2005).
[18] I. Puscasu and W. L. Schaich, Appl. Phys. Lett. **92**, 233102 (2008).
[19] S. Shen, A. Narayanaswamy, and G. Chen, Nano Lett. **9**, 2909 (2009).
[20] X. Liu, T. Tyler, T. Starr, A. F. Starr, N. M. Jokerst, and W. J. Padilla, Phys. Rev. Lett. **107**, 045901 (2011).
[21] M. De Zoysa, T. Asano, K. Mochizuki, A. Oskooi, T. Inoue, and S. Noda, Nat. Photonics **6**, 535 (2012).
[22] K. A. Arpin, M. D. Losego, A. N. Cloud, H. Ning, J. Mallek, N. P. Sergeant, L. Zhu, Z. Yu, B. Kalanyan, G. N. Parsons, G. S. Girolami, J. R. Abelson, S. Fan, and P. V. Braun, Nat. Commun. **4**, 2630 (2013).
[23] V. W. Brar, M. C. Sherrott, M. S. Jang, S. Kim, L. Kim, M. Choi, L. A. Sweatlock, and H. A. Atwater, Nat. Commun. **6**, 7032 (2015).
[24] R. H. Dicke, Phys. Rev. **93**, 99 (1954).
[25] M. Scheibner, T. Schmidt, L. Worschech, A. Forchel, G. Bacher, T. Passow, and D. Hommel, Nat. Phys. **3**, 106 (2007).
[26] R. Röhlsberger, K. Schlage, B. Sahoo, S. Couet, and R. Rüffer, Science **328**, 1248 (2010).
[27] J. G. Bohnet, Z. Chen, J. M. Weiner, D. Meiser, M. J. Holland, and J. K. Thompson, Nature **484**, 78 (2012).
[28] Q. Xu, S. Sandhu, M. L. Povinelli, J. Shakya, S. Fan, and M. Lipson, Phys. Rev. Lett. **96**, 123901 (2006).
[29] S. Zhang, D. A. Genov, Y. Wang, M. Liu, and X. Zhang, Phys. Rev. Lett. **101**, 047401 (2008).
[30] B. Luk'yanchuk, N. I. Zheludev, S. A. Maier, N. J. Halas, P. Nordlander, H. Giessen, and C. T. Chong, Nat. Mater. **9**, 707 (2010).
[31] A. E. Miroshnichenko, S. Flach, and Y. S. Kivshar, Rev. Mod. Phys. **82**, 2257 (2010).
[32] C. Wu, A. B. Khanikaev, R. Adato, N. Arju, A. A. Yanik, H. Altug, and G. Shvets, Nat. Mater. **11**, 69 (2012).
[33] V. N. Pustovit and T. V. Shahbazyan, Phys. Rev. Lett. **102**, 077401 (2009).
[34] D. Martín-Cano, L. Martín-Moreno, F. J. García-Vidal, and E. Moreno, Nano Lett. **10**, 3129 (2010).
[35] J. J. Choquette, K.-P. Marzlin, and B. C. Sanders, Phys. Rev. A **82**, 023827 (2010).
[36] R. Fleury and A. Alù, Phys. Rev. B **87**, 201101 (2013).
[37] See Supplemental Material at http://link.aps.org/supplemental/10.1103/PhysRevB.92.024302 for detailed simulation methods and theoretical derivation.
[38] W. Suh, Z. Wang, and S. Fan, IEEE J. Quantum Electron. **40**, 1511 (2004).
[39] L. Zhu, S. Sandhu, C. Otey, S. Fan, M. B. Sinclair, and T. S. Luk, Appl. Phys. Lett. **102**, 103104 (2013).
[40] S. Yi, M. Zhou, Z. Wang, and Z. Yu, Phys. Rev. B **89**, 195449 (2014).
[41] E. Prodan, C. Radloff, N. J. Halas, and P. Nordlander, Science **302**, 419 (2003).
[42] L. Verslegers, Z. Yu, P. B. Catrysse, and S. Fan, J. Opt. Soc. Am. B **27**, 1947 (2010).
[43] L. Verslegers, Z. Yu, Z. Ruan, P. B. Catrysse, and S. Fan, Phys. Rev. Lett. **108**, 083902 (2012).
[44] K. S. Miller, Math. Mag. **54**, 67 (1981).
[45] Z. Yu, A. Raman, and S. Fan, Phys. Rev. Lett. **109**, 173901 (2012).